



Cite this: *J. Mater. Chem. C*, 2019, 7, 13743

Received 30th August 2019,
Accepted 14th October 2019

DOI: 10.1039/c9tc04792a

rsc.li/materials-c

Efficient polymer light-emitting diodes (PLEDs) based on chiral [Pt(C[^]N)(N[^]O)] complexes with near-infrared (NIR) luminescence and circularly polarized (CP) light†

Guorui Fu,^{‡a} Yani He,^{‡a} Wentao Li,^a Baowen Wang,^a Xingqiang Lü,^{id}*^a
Hongshan He,^{id}*^b and Wai-Yeung Wong,^{id}*^{cd}

Based on the molecular design of the chiral NIR emitters [Pt(iqbt)-(S-Lⁿ)] (1–4), the first examples of CP-NIR-PLEDs with both attractive NIR-emission properties ($\lambda_{em} = 732$ nm; $\eta_{EGE}^{MAX} = 0.87$ – 0.93%) and high dissymmetry g_{EL} factors up to 10^{-3} are reported.

Circularly polarized (CP) light-active materials,¹ due to the tracking of their specific interactions with chiral environments, have recently attracted particular interest in the field of chiral optoelectronics.² CP organic/polymer light-emitting diodes (OLEDs/PLEDs)³ show the advantage of being able to directly generate CP light and have achieved high-contrast 3D images and true backlight, and are hence significantly superior to traditional OLEDs/PLEDs. To date, studies of small molecules⁴ or polymers⁵ with $^1\pi$ - π^* -transition fluorescence have been reported. The ability of thermally activated delayed fluorescence (TADF)⁶ systems, transition-metal complexes⁷ and organo-Ln³⁺ complexes⁸ to harvest both 1S and 1T excitons for vivid visible-light ($\lambda_{em} = 400$ – 700 nm) CP-OLEDs/PLEDs makes the resulting devices more appealing. In particular, the CP devices that emit in the near-infrared (NIR; $\lambda_{em} > 700$ nm) offer numerous advantages for bioassays, information security, and displays meant to be readable at night.⁹ However, few such studies have been pursued, which can be attributed to several challenges including apparently unavoidable aggregation of CP-active materials and the lack of NIR-active chiroptical luminogens.

Pt(II)-complex phosphors have, however, achieved great success in the development¹⁰ of efficient NIR-OLEDs/PLEDs. In this context, one elegant strategy toward that restrictive NIR regime for typical vacuum-deposited NIR-OLEDs is focused on the significant bathochromatic shift of sublimed Pt(II) complexes caused by the unforeseen formation of excimers and strong Pt...Pt intermolecular interactions. However, despite the issues of aggregation-induced quenching or enhancement of emission (AIQ or AIE),¹¹ the realization of η_{EQE} values up to 1%¹² or even double figures¹³ actually makes up for the inevitable high cost of the device fabrication and the detrimental aggregation-induced efficiency roll-off. Solution-processable NIR-OLEDs/PLEDs¹⁴ based on homogeneous doping of a Pt(II) complex displaying a strong metal-to-ligand charge-transfer (MLCT) effect into an appropriate host with a deep HOMO–LUMO bandgap have been convincingly shown to circumvent such problems, and have specifically been shown to be cost effective and display desirable device performance (high efficiency with relatively low efficiency roll-off), and should hence be more seriously considered as an alternative. In contrast, the development of highly emissive NIR-OLEDs/PLEDs without Pt(II)-chromophore interactions remains a great challenge due to the “energy gap law”¹⁵ limit. Nuzzo *et al.*¹⁶ used a chirally substituted polymer doped with an achiral Pt(II) complex as the emitting material and fabricated using this material a device displaying emission of light at a wavelength of about 550 nm. Fuchter *et al.*¹⁷ incorporated a chiral Pt(II) complex into a conventional light-emitting polymer and the CP electroluminescence was observed at a wavelength of about 600 nm. In light of the promising NIR ($\lambda_{em} = 707$ nm) emission¹⁸ of [Pt(iqbt)(dpm)] (Scheme 1), we developed in the current work the first example of CP-NIR-PLEDs by introducing simple chirality into the N[^]O-Schiff-base ancillary ligands **S-HLⁿ** ($n = 1$ – 4) for the purpose of synthesizing their corresponding chiral [Pt(iqbt)(S-Lⁿ)]-heteroleptic complexes (1–4; see also Scheme 1). Both CP-light activity and NIR electroluminescence (732 nm) were observed. This result demonstrated the potential application of chiral NIR-light-emitting Pt(II) complexes in solution-processable CP-NIR-PLEDs.

^a School of Chemical Engineering, Shaanxi Key Laboratory of Degradable Medical Material, Northwest University, Xi'an 710069, Shaanxi, China.

E-mail: lvxq@nwu.edu.cn; Fax: +86-29-88302312; Tel: +86-29-88302312

^b School of Chemistry, Eastern Illinois University, Charleston, IL 61920, USA.

E-mail: hhe@eiu.edu

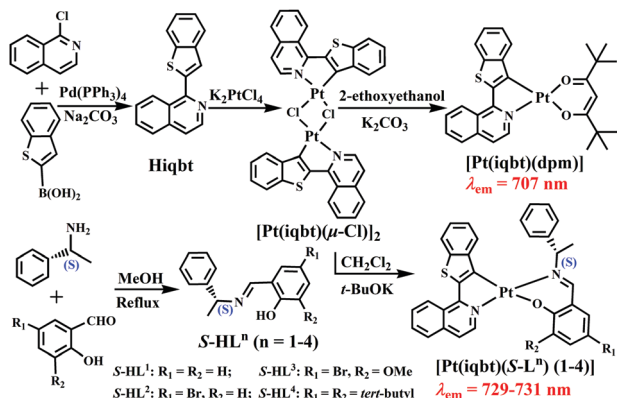
^c Department of Applied Biology and Chemical Technology, The Hong Kong Polytechnic University, Hung Hom, Hong Kong, P. R. China.

E-mail: wai-yeung.wong@polyu.edu.hk

^d Hong Kong Polytechnic University Shenzhen Research Institute, Shenzhen 518057, China. E-mail: wai-yeung.wong@polyu.edu.hk

† Electronic supplementary information (ESI) available: Starting materials and characterization; and XRD, UV, and PL data. CCDC 1941079. For ESI and crystallographic data in CIF or other electronic format see DOI: 10.1039/c9tc04792a

‡ These authors contributed equally and should be considered co-first authors.



Scheme 1 Synthetic scheme for the chiral Schiff-base ligands **S-HLⁿ** ($n = 1-4$) and their Pt(II) complexes **[Pt(iqbt)(S-Lⁿ)]** ($n = 1-4$).

Based on the reaction (also Scheme 1) of K_2PtCl_4 with the C^N-cyclometalated ligand **Hiqbt** synthesized from the Suzuki coupling of cost-effective 2-Cl-isoquinoline¹⁹ with benzo[*b*]thien-2-yl boronic acid, the μ -chloro-bridged dimer intermediate **[Pt(iqbt)(μ -Cl)]₂** was obtained in 89% yield. The chiral Schiff-base-type ligands **S-HLⁿ** ($n = 1-4$) were prepared from the rational condensation²⁰ of *S*(-)-1-phenylethylamine with the appropriate salicylaldehyde derivatives, respectively. Furthermore, through the treatment of **[Pt(iqbt)(μ -Cl)]₂** with each of the chiral ligands **S-HLⁿ** ($n = 1-4$) in the presence of *t*-BuOK, the targeted chiral Pt(II) complexes **[Pt(iqbt)(S-Lⁿ)]** (**1-4**), each soluble in common organic solvents, were afforded, respectively.

The chiral Schiff-base-type ligands **S-HLⁿ** ($n = 1-4$) and their Pt(II) complexes **1-4** were well characterized using EA, FT-IR, ¹H NMR (Fig. S1 and S2, ESI[†]) and ESI-MS. All of the Pt(II) complexes exhibited relatively high thermal stabilities. TGA results (Fig. S3, ESI[†]) of the chiral Pt(II) complexes **1-4** showed them to display high decomposition temperatures (T_d values corresponding to 5% weight loss of 230 °C for **1**, 267 °C for **2**, 239 °C for **3** and 214 °C for **4**). The relatively favourable thermal stability of **2** with its electron-withdrawing Br atom, and the relatively poor thermal stability of **4** with its electron-donating *tert*-butyl groups, can be reasonably explained by the relatively shorter Pt-C (1.99421 Å), Pt-N (2.05599–2.06234 Å) and Pt-O (2.11856 Å) bond lengths (Table S1, ESI[†]) for **2** than for **4** (Pt-C (2.00438 Å), Pt-N (2.05585–2.06706 Å) and Pt-O (2.12124 Å)), determined from the TD-DFT calculations described below. The molecular structure of **[Pt(iqbt)(S-L³)]** (**3**) was confirmed using X-ray single-crystal diffraction analysis. The complex crystallized in the triclinic space group *P1*, and its non-centrosymmetric nature originated from the (S-L³)⁻-induced chirality. As shown in Fig. 1, one C11^{N1}-chelating (iqbt)⁻ ligand and one ancillary ligand (S-L³)⁻ with the N2^{O2}-chelate mode coordinated to the central Pt²⁺ ion (Pt1) in a square planar geometry, leading to the formation of a typical asymmetric mononuclear framework.¹⁸ Noticeably, in contrast to the co-planar conformation of the cyclometalated (iqbt)⁻ ligand, the terminal phenyl ring of the chiral (S-L³)⁻ ligand was observed to be almost perpendicular to its N2^{O2}-chelation plane with a dihedral angle of 84.1(2)°, for which the *S*-chiroptical character centered at the chiral -C*24-H

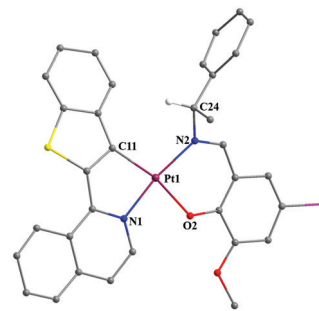


Fig. 1 A perspective drawing of the mononuclear framework of the chiral **[Pt(iqbt)(S-L³)]** (**3**); H atoms are omitted for clarity.

atom for **[Pt(iqbt)(S-L³)]** (**3**) was well retained. Interestingly, complementary intermolecular interactions (3.566(2) Å, 3.791(2) Å, and 3.710(30) Å for a $\pi \cdots \pi$, $\pi \cdots Pt$, and C18–H18 $\cdots \pi$ interactions, respectively; Fig. S4, ESI[†]) but no valid Pt \cdots Pt interactions were observed between every adjacent two mononuclear units, giving rise to the 1D polymeric chain. The crystallographic data for this compound are provided in Tables S2 and S3 (ESI[†]).

Photophysical properties of the chiral Pt(II) complexes **1-4** in solution and the solid state were explored at RT and 77 K (Table S4 and Fig. 2, 3 and Fig. S5–S9, ESI[†]). As shown in Fig. 2,

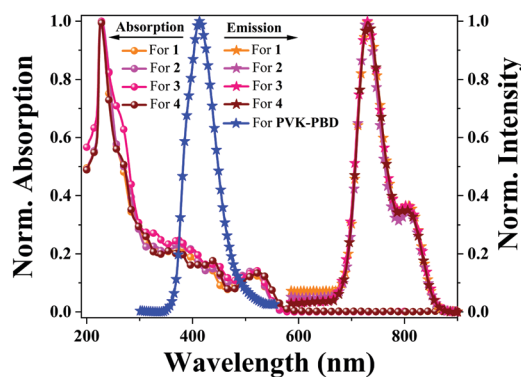


Fig. 2 The acquired normalized UV-visible absorption and emission spectra of the chiral Pt(II) complexes **1-4** in degassed solution and of PVK-PBD in the solid state, all at RT.

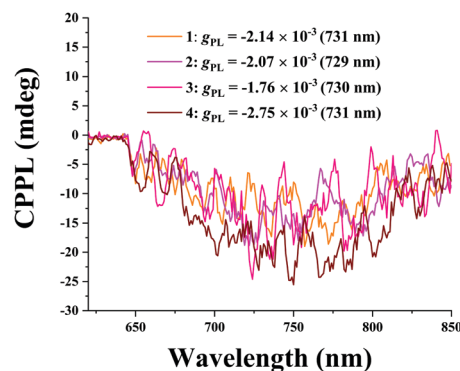


Fig. 3 The CP light spectra of the chiral Pt(II) complexes **1-4** in degassed solution at RT.

chiral Pt(II) complexes **1–4** in solution showed significantly broader UV-visible absorption spectra peaks ($\lambda_{\text{ab}} < 400$ nm; Fig. S5, ESI†) than did the **Hiqbt** and **S-HLⁿ** ligands: the high-energy-state intense absorption in the 200–400 nm range was assigned to the ligand-based $^1\pi-\pi^*$ transitions, and the relatively weak absorptions at $\lambda_{\text{ab}} > 430$ nm were probably due to a mixture of $^1,^3\text{LLCT}$ and $^1,^3\text{MLCT}$ transitions. The substituents on the (**S-Lⁿ**)[−] ligands displayed little effect on the absorption and CD spectra (Fig. S6, ESI†) of their Pt(II) complexes. Importantly, in contrast to the ligand-related visible-light emissions (Fig. S7, ESI†) from both the **Hiqbt** and **S-HLⁿ** ligands, all four chiral Pt(II) complexes **1–4** in solution at RT emitted, uniquely, NIR light, as shown in Fig. 2, with specifically a strong peak located at $\lambda_{\text{em}} = 730$ nm and a shoulder at 806 nm. Of these two emission features (which were attributed to 0–0 and 0–1 transitions, respectively), as a result of different degrees of vibrational coupling, the lower-energy emission feature was probably made up of high-frequency normal modes with larger Huang–Rhys factors.²¹ Their phosphorescences showed a short lifetime of 0.88 μs for **1**, and significantly longer lifetimes of 1.02 μs for **2** and 0.96 μs for **3**, the latter two of which were probably due to Br-facilitated intersystem-crossing. The shortest lifetime, 0.85 μs , was found for **4** and was probably due at least in part to the electron-donating effects of two *tert*-butyl groups. It is worth noting that the NIR-light-emission efficiency (Φ_{PL}) values of all four chiral Pt(II) complexes were also controlled by the (**S-Lⁿ**)[−]-involved electronic effects – and that their Φ_{PL} values centered at 731 nm, more attractive than those of the reported NIR-light-emitting Pt(II) complexes¹⁰ just with the MLCT impact, were attributed to their large radiative rate constant ($k_{\text{r}} = 10^5 \text{ s}^{-1}$). The Br-containing chiral Pt²⁺ complex **2** gave rise to the best NIR-emission Φ_{PL} of 21%, which was due to its displaying the highest k_{r} ($2.10 \times 10^5 \text{ s}^{-1}$) and lowest k_{nr} ($7.75 \times 10^5 \text{ s}^{-1}$). The effective radiative transition with the weak vibrational coupling for the four chiral Pt²⁺ complexes **1–4** was further confirmed by the results of their rigidochromic shifts (Fig. S8, ESI†) at 77 K, whereas the (**S-Lⁿ**)[−]-incorporation benefited from effectively side-stepping the intramolecular rotation/distortion for more of a chance to realize the T₁-preferred radiative decay with longer phosphorescence lifetimes. Slight blue shifts ($\lambda_{\text{em}} = 725\text{--}727$ nm) for **1–2** and red shifts ($\lambda_{\text{em}} = 741\text{--}751$ nm) for **3–4** were observed in the solid state (Fig. S9, ESI†) relative to that ($\lambda_{\text{em}} = 732$ nm) in solution at RT, and these results were probably due to strong intermolecular interactions (see also Fig. S4, ESI†) as in the case of traditional Pt²⁺ complexes.

Their CD spectra (see also Fig. S6, ESI†) showed the Cotton effects with two positive signals at 259–268 and 328–331 nm and a negative one at 286–313 nm as has been observed for the free **S-HLⁿ** ligands, but also showed additional broad Cotton-effect bands arising from the (**S-Lⁿ**)[−]-controlled exciton-coupled $^1,^3\text{LLCT}/^1,^3\text{MLCT}$ transitions with three negative signals and two positive signals between 355 nm and 600 nm. The emission dissymmetry factor (g_{PL}) values (Fig. 3) of the four (**S-Lⁿ**)[−]-involved chiral Pt(II) complexes were all on the order of 10^{-3} (specifically -2.14×10^{-3} (731 nm) for **1**; -2.07×10^{-3} (729 nm) for **2**; -1.76×10^{-3} (730 nm) for **3**, and -2.75×10^{-3} (731 nm) for **4**), indicative of an (**S-Lⁿ**)[−] control of the intensity

of corresponding NIR light emission peak, probably due to different levels of electron cloud sharing²² especially within the chiral (**S-Lⁿ**)[−] portion (see also Table S4 and Fig. S10, ESI†).

Theoretical studies were also carried out, and they provided further insights into the photophysical properties of these chiral complexes [Pt(**iqbt**)(**S-Lⁿ**)] (**1–4**). TD-DFT calculations (Table S5 and Fig. S10, ESI†) indicated that the chiral Pt(II) complexes **1–4** displayed similar LUMO+1 as well as LUMO electron density distribution patterns, with most (90.20–93.04%) of the LUMO+1 electron density contributed by the (**S-Lⁿ**)[−] ligand and most (90.40–90.68%) of the LUMO electron density from the (**iqbt**)[−] ligand. The HOMO electron density was also predominantly from the ligands, with more from the (**iqbt**)[−] ligand (43.90%) than from the (**S-L¹**)[−] ligand (38.36%) for **1**, but more from the (**S-Lⁿ**)[−] ($n = 2\text{--}4$) ligand for **2–4** (47.81% for **2**, 59.87% for **3** and 60.48% for **4**). The introduction of the 3-position MeO/*tert*-butyl and/or 5-position Br/*tert*-butyl groups in **2–4** appeared to have resulted in the observed preferred contribution (53.47% for **2**, 62.32% for **3** or 63.88% for **4**) of the (**iqbt**)[−] ligand to their HOMO–1 electron densities. The introduction of the Br ligand appeared to have substantially destabilized both the HOMOs and LUMOs while the introduction of MeO- and *tert*-butyl groups appeared to have stabilized them. Hence, relatively narrow HOMO–LUMO bandgaps were observed for **2–4** (2.86 eV for **2**; 2.83 eV for **3** or 2.80 eV for **4**) relative to that of **1** (2.91 eV). Even though the calculated HOMO → LUMO transition (at 514 nm for **1**; 524 nm for **2**; 526 nm for **3** and 532 nm for **4**) came mainly (over 97%) from the S₀ → S₁ transition, the experimentally determined lower-energy ($\lambda_{\text{ab}} > 430$ nm; 518–521 nm for **1–4**) absorptions probably also included the LLCT/MLCT transitions. NTO calculations (Table S6 and Fig. S11, ESI†) for S₀ → T₁ excitations indicated that about 80% of the hole orbital was contributed by (**S-Lⁿ**)[−] and 92% of the particle orbital was from the (**iqbt**)[−] ligand for each of the chiral Pt(II) complexes **1–4**, forming almost the entire (*ca.* 99%) hole → particle transition, and hence suggesting that the $^3\text{LLCT}$ -dominated transitions and the less prevalent $^3\text{MLCT}$ transitions were responsible for their NIR-light-emission phosphorescences. These bandgaps were found to be quite similar to those determined electrochemically (Fig. S12 and also Table S4, ESI†).

Of particular interest are the cost-effective and large-area flexible CP-NIR-PLEDs based on these chiral Pt(II) complexes **1–4**. PVK-PBD was used as the host due to its good hole-electron transport, and the significant spectral overlap (also Fig. 2) between the emission of light from PVK-PBD and the LLCT/MLCT absorption of light by the chiral Pt(II) complexes **1–4**, features beneficial for effective Förster energy transfer²³ from PVK-PBD to the chiral Pt(II)-complex species. Since the LUMO (−2.95 to −2.86 eV) and HOMO (−5.66 to −5.61 eV) levels of the chiral Pt(II) complexes **1–4** fit perfectly within those (−2.50 to −2.00 eV of LUMOs and −6.10 to −5.50 eV of HOMOs) of PVK and PBD, respectively, the injected holes from PEDOT:PSS and the injected electrons from TPBi would pass through the PVK-PBD host to be trapped by the chiral Pt(II)-complex species, and subsequently direct charge carrier trapping and recombination

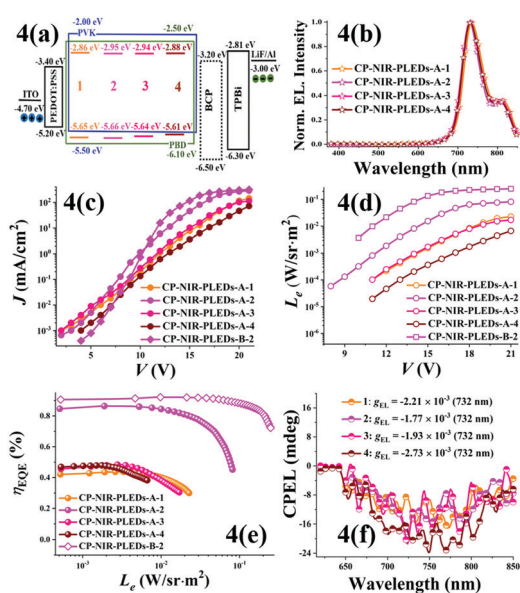


Fig. 4 (a) Device structures and energy level diagrams. (b) Normalized electroluminescence spectra. (c) J - V , (d) L_e - V , (e) η_{EQE} - L_e , and (f) g_{EL} curves based on **NIR-CP-PLEDs-A/B** from the chiral Pt(II) complexes **1-4**.

should take place. Through the solution-processable procedure with the same configuration shown in Fig. 4(a), a series of **CP-NIR-PLEDs-A/B** using the chiral Pt(II) complexes **1-4** as the dopants with an intended doping level of 8 wt% were fabricated. The difference between the A and B series was that a hole-blocking BCP layer was added in the B series.

As shown in Table S7 (ESI^\dagger) and Fig. 4(b)/Fig. S13 (ESI^\dagger), all of the normalized electroluminescence NIR-emission ($\lambda_{\text{em}} = 732 \text{ nm}$) spectra for the **CP-NIR-PLEDs-A** series well resembled those of the chiral Pt(II) complexes **1-4** in solution at RT, with this similarity due to the low-concentration dispersion of the dopants **1-4** into the corresponding PVK-PBD host together with the absence of the above-described strong intermolecular interactions (see also Fig. S4, ESI^\dagger). The spectra also showed featureless structures and independence of the applied bias voltage. Fig. 4(c-e) show the J - V , L_e - V and η_{EQE} - L_e curves for **CP-NIR-PLEDs-A** with the different chiral Pt(II) complexes **1-4**. In contrast to the monotonously increasing values of J and L_e with increasing applied bias voltage, η_{EQE} in each case increased initially and then instantly decreased throughout the corresponding illumination. The highest device efficiency was observed for the **CP-NIR-PLED-A-2** device, which showed an $\eta_{\text{EQE}}^{\text{Max}}$ of 0.87% with $L_e = 0.002 \text{ W sr}^{-1} \text{ m}^{-2}$ at $J = 6.02 \text{ mA cm}^{-2}$ after 10.5 V of the V_{on} (the voltage of $L_e = 5 \times 10^{-4} \text{ W sr}^{-1} \text{ m}^{-2}$). In comparison, both the $\eta_{\text{EQE}}^{\text{Max}}$ and L_e^{Max} values (0.44–0.49% and 0.007 – $0.023 \text{ W sr}^{-1} \text{ m}^{-2}$) of all the other **CP-NIR-PLEDs-A** devices based on chiral Pt(II) complexes **1** and **3-4** were lower than those (0.87% and $0.081 \text{ W sr}^{-1} \text{ m}^{-2}$) of the **CP-NIR-PLED-A-2**, consistent with the measured order of their Φ_{PL} results afforded by the $(\text{S-L}^{\text{M}})^-$ -involved electronic effect for their chiral Pt(II) complexes (**1-4**) in solution (see also Table S4, ESI^\dagger). Nonetheless, the T_1 -decay-involved phosphorescence lifetime being longest for the $(\text{S-L}^{\text{M}})^-$ -induced **2** with the electron-withdrawing

effect of the 5-position Br resulted in **CP-NIR-PLED-A-2** displaying a significantly higher efficiency roll-off (48%) than did of the other three devices (20–37%). For optimization, **CP-NIR-PLED-B-2** (see also Fig. 4(a)) with an additional hole-blocking BCP layer was fabricated. Delightfully, due in part to a greater number of excitons confined within the broadened recombination zone,²⁴ a distinctively improved NIR-emission electroluminescence (see also Fig. 4(b-e)) was achieved. First, despite using an illumination voltage of only 6.0 V, the L_e^{Max} was almost three times higher than that of the **CP-NIR-PLED-A-2**. Moreover, the reformed carrier balance within the **CP-NIR-PLED-B-2** also endowed it with an $\eta_{\text{EQE}}^{\text{Max}}$ of up to 0.93%, attractive relative to those of previously described Pt(II)-complex-based NIR-PLEDs.^{10,14} Interestingly enough, its efficiency roll-off (23%) was also relieved. Worthy of notice, as shown in Fig. 4(f), the dissymmetry factors (g_{EL} , see also Table S7, ESI^\dagger) of all of the **CP-NIR-PLEDs** were also on the order of 10^{-3} (determined by $(\text{S-L}^{\text{M}})^-$), similar to those of the previously reported Pt(II)-complex-based visible CP-OLEDs.⁷

In conclusion, through the involvement of $(\text{S-L}^{\text{M}})^-$ - N°O ancillary ligands with different electronic effects, a series of chiral $[\text{Pt}(\text{iqbt})(\text{S-L}^{\text{M}})]$ complexes (**1-4**) displaying emission of NIR light ($\lambda_{\text{em}} = 729$ – 731 nm) and CPL-active properties were obtained. Moreover, as a result of their being doped into the PVK-PBD host, the resulting **CP-NIR-PLEDs** showed quite attractive device performance measures ($\lambda_{\text{em}} = 732 \text{ nm}$; $\eta_{\text{EQE}}^{\text{Max}}$ up to 0.87–0.93%) and high g_{EL} of up to 10^{-3} , features observed for the first time to the best of our knowledge. This result suggested that the $(\text{S-L}^{\text{M}})^-$ -involved chiral $[\text{Pt}(\text{iqbt})(\text{S-L}^{\text{M}})]$ complexes are promising candidates for future **CP-NIR-PLEDs**.

Conflicts of interest

There are no conflicts to declare.

Acknowledgements

This work was supported by the NNSF (21373160, 21173165), the Wisteria Scientific Research Cooperation Special Project of Northwest University, and the NSF (1507871) of the USA.

Notes and references

- 1 E. M. Sánchez-Carnerero, A. R. Agarrabeitia, F. Moreno, B. L. Maroto, G. Muller, M. J. Ortiz and S. de la Moya, *Chem. – Eur. J.*, 2015, **21**, 13488–13500.
- 2 Y. J. Zhang, T. Oka, R. Suzuki and J. T. Ye, *Science*, 2014, **344**, 725–728.
- 3 J. M. Han, S. Guo, H. Lu, S. J. Liu, Q. Zhao and W. Huang, *Adv. Opt. Mater.*, 2018, **6**, 1800538.
- 4 (a) M. Shimada, Y. Yamanoi, T. Ohto, S. T. Pham, R. Yamada, H. Tada, K. Omoto, S. Tashiro, M. Shionoya and M. Hattori, *J. Am. Chem. Soc.*, 2017, **139**, 11214–11221; (b) H. Sakai, S. Shinto, J. Kumar, Y. Araki, T. Sakanoue, T. Takenobu, T. Wada, T. Kawai and T. Hasobe, *J. Phys. Chem. C*, 2015, **119**, 13937–13947.

- 5 (a) D. M. Lee, J. W. Song, Y. J. Lee, C. J. Yu and J. H. Kim, *Adv. Mater.*, 2017, **29**, 1700907; (b) Y. Yang, R. Correa da Costa, D. M. Smilgies, A. J. Campbell and M. J. Fuchter, *Adv. Mater.*, 2013, **25**, 2624–2628.
- 6 (a) M. Li, S. H. Li, D. D. Zhang, M. H. Cai, L. Duan, M. K. Fung and C. F. Chen, *Angew. Chem., Int. Ed.*, 2018, **57**, 2889–2893; (b) S. Feuillastre, M. Pauton, L. H. Gao, A. Desmarchelier, A. J. Riives, D. Prim, D. Tondelier, B. Gffroy, G. Muller and G. Clavier, *J. Am. Chem. Soc.*, 2016, **138**, 3990–3993.
- 7 M. Ibrahim-Ouali and F. Dumur, *Molecules*, 2019, **24**, 1412.
- 8 (a) F. Zinna, M. Pasini, F. Galeotti, C. Botta, L. Di Bari and U. Giovanella, *Adv. Funct. Mater.*, 2017, **27**, 201603719; (b) F. Zinna, U. Giovanella and L. Di Bari, *Adv. Mater.*, 2015, **27**, 1791–1795.
- 9 (a) Z. Guo, S. Park, J. Yoon and I. Shin, *Coord. Chem. Rev.*, 2014, **43**, 16–29; (b) H. F. Xiang, J. H. Cheng, X. F. Ma, X. G. Zhu and J. J. Jason, *Chem. Soc. Rev.*, 2013, **42**, 6128–6185.
- 10 (a) Y. M. Zhang, Y. F. Wang, J. Song, J. L. Qu, B. H. Li, W. G. Zhu and W.-Y. Wong, *Adv. Opt. Mater.*, 2018, **6**, 1800466; (b) C.-L. Ho, H. Li and W.-Y. Wong, *J. Organomet. Chem.*, 2014, **751**, 261–285.
- 11 (a) K. Kenda and S. Kazuki, *Angew. Chem., Int. Ed.*, 2019, **58**, 8632–8639; (b) M. Ju, Y. Hong, W. Y. Jacky, A. J. Qin, Y. H. Tang and B. Z. Tang, *Adv. Mater.*, 2014, **26**, 5429–5479.
- 12 (a) F. Nisic, A. Colombo, C. Dragonetti, D. Roberto, A. Valore, J. M. Malicka, M. Cocchi, G. R. Freeman and J. A. G. Williams, *J. Mater. Chem. C*, 2014, **2**, 1791–1800; (b) E. Rossi, A. Colombo, C. Dragonetti, D. Roberto, F. Demartin, M. Cocchi, P. Brulatti, V. Fattori and J. A. G. Williams, *Chem. Commun.*, 2012, **48**, 3182–3184.
- 13 (a) X. L. Yang, H. R. Guo, X. B. Xu, Y. H. Sun, G. J. Zhou, W. Ma and Z. X. Wu, *Adv. Sci.*, 2019, **6**, 1801930; (b) K. Tuong, Ly, R.-W. Chen-Chen, H.-W. Lin, Y.-J. Shiau, S.-H. Liu, P.-T. Chou, C.-S. Tsao, Y.-C. Huang and Y. Chi, *Nat. Photonics*, 2017, **11**, 63–68.
- 14 (a) Z. R. Hao, F. Y. Meng, P. Wang, Y. F. Wang, H. Tan, Y. Pei, S. J. Su and Y. Liu, *Dalton Trans.*, 2017, **46**, 16257–16268; (b) Y. M. Zhang, Z. Yin, F. Y. Meng, J. T. Yu, C. F. You, S. Y. Yang, H. Tan, W. G. Zhu and S. J. Su, *Org. Electron.*, 2017, **50**, 317–324; (c) N. Su, F. Y. Meng, P. Wang, X. Liu, M. B. Zhu, W. G. Zhu, S. J. Su and J. T. Yu, *Dyes Pigm.*, 2017, **138**, 162–168; (d) W. J. Xiong, F. Y. Meng, H. Tan, Y. F. Wang, P. Wang, Y. M. Zhang, Q. Tao, S. J. Su and W. G. Zhu, *J. Mater. Chem. C*, 2016, **4**, 6007–6015; (e) K. R. Graham, X. Y. Yang, J. R. Sommer, A. H. Shelton, K. S. Schanze, J. G. Xue and J. R. Reynolds, *Chem. Mater.*, 2011, **23**, 5305–5312; (f) J. R. Sommer, R. T. Farley, K. R. Graham, X. Y. Yang, J. R. Reynolds, J. G. Xue and K. S. Schanze, *ACS Appl. Mater. Interfaces*, 2009, **1**, 274–278.
- 15 Z. Andrea, M. Alessandro and C. Franco, *Adv. Funct. Mater.*, 2019, **29**, 1807623.
- 16 D. Di Nuzzo, C. Kulkarni, B. D. Zhao, E. Smolinsky, F. Tassinari, S. C. J. Meskers, R. Naaman, E. W. Meijer and R. H. Eriend, *ACS Nano*, 2017, **11**, 12713–12722.
- 17 Y. Yang, R. Correa da Costa, D. Smilgies, A. J. Campbell and M. J. Fuchter, *Adv. Mater.*, 2013, **25**, 2624–2628.
- 18 M. Penconi, M. Cazzaniga, S. Kesarkar, P. R. Mussini, D. Ceresoli and A. Bossi, *Photochem. Photobiol. Sci.*, 2017, **16**, 1220–1229.
- 19 (a) J. Zhou, G. R. Fu, Y. N. He, L. N. Ma, W. T. Li, W. X. Feng and X. Q. Lü, *J. Lumin.*, 2019, **209**, 427–434; (b) G. R. Fu, H. Zheng, Y. N. He, W. T. Li, X. Q. Lü and H. S. He, *J. Mater. Chem. C*, 2018, **6**, 10589–10596.
- 20 A. C. Chamayou, S. Ludeke, V. Brecht, T. B. Freedman, L. A. Nafie and C. Janiak, *Inorg. Chem.*, 2011, **50**, 11363–11374.
- 21 W. L. Cai, A. C. Zhao, K. Ren, R. X. He, M. Li and W. Shen, *J. Phys. Chem. C*, 2019, **123**, 17968–17975.
- 22 Z. P. Yan, K. Liao, H. B. Han, J. Su, Y. X. Zheng and J. L. Zuo, *Chem. Commun.*, 2019, **55**, 8215–8218.
- 23 F. N. Castellano, *Acc. Chem. Res.*, 2015, **48**, 828–839.
- 24 T. Mori, Y. Masumoto and T. Itoh, *J. Photopolym. Sci. Technol.*, 2008, **21**, 173–180.